Investigations on High Reynolds Number Laminar Flow Airfoils

G. Redeker,* K. H. Horstmann,† H. Köster,† and A. Quast†
German Aerospace Research Establishment (DFVLR), Braunschweig, Federal Republic of Germany

For further operating-cost reduction on transport aircraft, drag reduction by extended laminar flow on wings and empennages is mandatory. With carefully designed airfoils, laminar flow can be achieved even at high Mach and Reynolds numbers and moderate sweep angles. With laminar airfoils the fuel consumption decreases on the order of 30%. Two- and three-dimensional stability theory seems to be a good tool for determining laminar-turbulent boudary-layer transition caused by Tollmien-Schlichting and crossflow instabilities, but it must be checked by extensive flight tests.

Nomenclature

c	= airfoil chord length, m
c_d	= drag coefficient-airfoil
c_l	= lift coefficient-airfoil
c_L	= lift coefficient-wing
c_p	= pressure coefficient
L/D	= lift to drag ratio
M	= Mach number
M_F	= flight Mach number
N_{CFI}	= amplification exponent for crossflow instability
N_{TSI}	= amplification exponent for Tollmien-Schlichting instabilty
Re	= Reynolds number
U_e	= stream velocity at the boundary layer edge, m/s
V_∞	= undisturbed flow velocity, m/s
x	= streamwise coordinate, m
x/c	= fraction of chord
y	= coordinate perpendicular to streamlines, m
z	= coordinate perpendicular to wing surface, m
α	= angle of attack, deg
Λ	= aspect ratio of wing
φ	= sweep angle, deg

I. Introduction

INCREASING fuel prices in the past and the long-term forecast of further rising energy costs, together with strong competition among the airlines, are the incentives for the development of new commercial transport aircraft with remarkable reduction in fuel consumption and increased economic operation. Through new technologies in aerodynamics, drag reduction is possible by increasing the length of the laminar boundary layer on a wing surface, thus reducing skin friction drag considerably. Low drag airfoils or laminar airfoils have been used extensively for years in gliders, and very low drag coefficients have been achieved compared to those of conventional airfoils used for transport aircraft, as demonstrated in Fig. 1, where two drag polars of different airfoils are compared. The first is the laminar airfoil DFVLR-HQ35, designed for a glider, and the second is the transonic airfoil DFVLR-R4, well suited for a transport aircraft. The extremely low drag coefficient c_d of the glider airfoil is mainly due to the reduction of skin friction by long extension of laminar boundary layers on upper and lower airfoil surface. This long extension of the laminar boundary layer is promoted by specially tuned pressure distributions and by the low Reynolds numbers ($Re \approx 2 \cdot 10^6$) of gliders. Airfoils for transonic aircraft operate at substantially higher Reynolds and Mach numbers and exhibit pressure distributions which have been designed according to transonic flow. When combined with Reynolds numbers of $Re \approx 20 \cdot 10^6$ and swept wings, these pressure distributions lead to fully turbulent boundary layers, resulting in a higher drag coefficient. From Fig. 1 it can be seen that the drag coefficient c_d of the glider airfoil is only 40% that of the transonic airfoil in a reasonable region of lift coefficients. The present paper deals with the possibility of extending the technology of natural laminar flow to higher Reynolds and Mach numbers and to the case of swept wings. In the following paper, a short description of the transition mechanisms from laminar to turbulent boundary layers on swept wings will be given, and the methods used for designing such airfoils will be outlined, including guidelines for the design. A design example will be discussed, together with the resulting improvement for a transport aircraft. Finally, some of the problems arising with this new technology will be addressed.

II. Transition from Laminar to Turbulent Boundary Layers on Swept Wings

Studies of economical operations of transport aircraft show that a high value of cruise speed times lift/drag ratio is necessary. As the lift/drag ratio of transport aircraft is nearly inde-

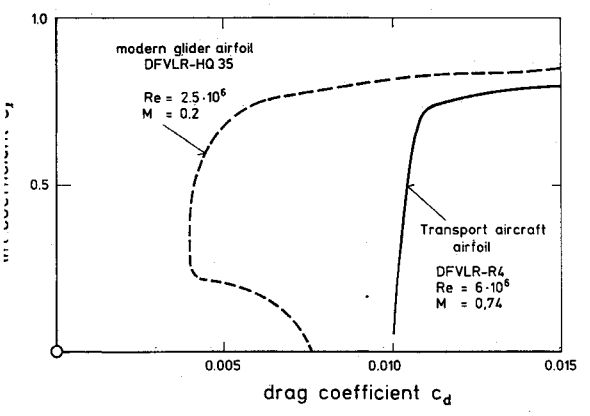

Fig. 1 Comparison of drag polars between airfoils of present transport aircraft and modern gliders.

Presented as Paper 86-1.1.3 at the 15th Congress of the International Council of Aeronautical Sciences, London, England, Sept. 7–12, 1986; received Sept. 26, 1986; revision received July 31, 1987.

*Head, Division of Airframe Aerodynamics, Institute for Aerodynamics.
†Research Engineer, Institute of Aerodynamics.

pendent from the cruise speed, (as long as no undesirable transonic effects occur), the highest velocity possible is the basis for a good economic operation. This leads to swept wing planforms for transonic transport aircraft.

Due to the sweep angle, the boundary layer on swept wings becomes highly three-dimensional, and additional effects can cause boundary-layer transition. Figure 2 gives an overview of the flowfield in the boundary layer of a swept wing. In the simple case of an infinite swept wing, the incoming flow can be split up into a spanwise component and a normal component. The flow component in the spanwise direction remains constant over the wing, forming an attachment line at the leading edge with a finite velocity. The streamlines of potential flow over the wing are highly curved in the planform plane at the leading edge region as a result of pressure gradients acting transversely to the local flow direction. Due to the presence of a boundary layer with zero velocity at the wing surface, the curvature of the wall streamlines is different from that of the potential flow, as is indicated in Fig. 2 by the full and dotted lines. This behavior leads to skewed velocity profiles in the boundary layer, where the flow direction changes as distance to the wall increases, from the direction of the wall streamline to the direction of the potential flow streamline. Splitting up these velocity profiles, in the direction of outer flow and perpendicular to it, yields the two velocity profiles also given in Figs. 2c and 2d. The first profile, in the direction of the outer flow, is very similar to that of a two-dimensional boundary layer, whereas the second one shows a different shape. This so-called crossflow distribution is characterized by a maximum near the surface, decreasing to zero velocity at the surface and at the outer edge of the boundary layer, including always a point of inflection.

These complicated flow patterns in the boundary layer, especially in the leading edge region, influence the transition of the laminar boundary layer on swept wings considerably. Essentially the following three transition mechanisms, or combinations of them, can occur:

1) Transition due to Tollmien-Schlichting instability (TSI), as known from the two-dimensional case,
2) transition due to crossflow instability (CFI),
3) attachment line transition (ALT).

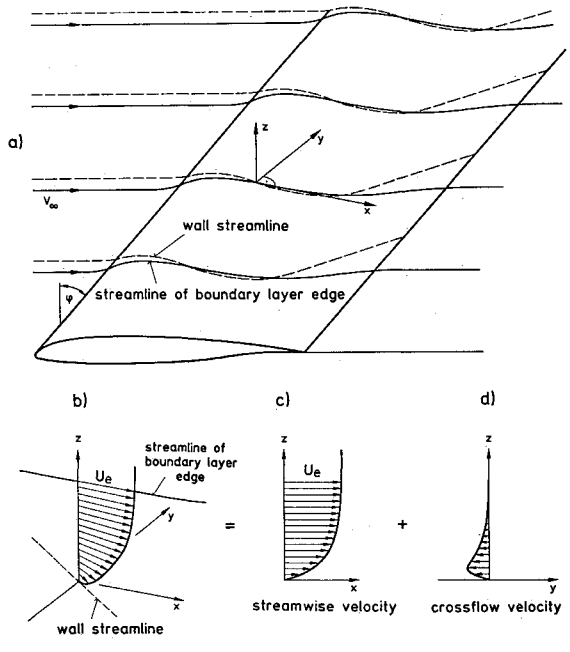

Fig. 2 Flow pattern and boundary-layer velocity distribution on an infinite swept wing: a) flow pattern; b) 3 dimensional velocity profile; c) streamwise velocity profile; d) crossflow velocity profile.

The boundary-layer profile in the direction of the outer flow is very similar to that of a two-dimensional boundary layer and, therefore, Tollmien-Schlichting waves[1] can occur which lead, through a complicated process, to transition into a turbulent boundary layer. The main parameters which influence the occurrence of unstable oscillations are pressure distribution and Reynolds number.

Early experiments on swept wings[2–4] showed a premature transition near the leading edge on smooth swept wings, and detailed investigations indicated that the instability of the crossflow velocity profiles caused boundary-layer transition. As these velocity profiles always have an inflection point, one can show from stability analysis considerations that the instability of such types of profiles is larger than usual.[5] The main parameters which influence the crossflow instability are sweep angle, Reynolds number, and pressure distribution.

Within the boundary layer of the attachment line flow, spanwise turbulent contamination can occur,[6,7] induced by an inherent instability of the boundary layer or by leading edge roughness. This behavior results in a fully turbulent boundary layer over the whole wing surface. Attachment line transition is dependent on sweep angle, Reynolds number, and acceleration of the flow in the attachment line region. Criteria for avoiding this kind of transition have been reported.[6,7] Crossflow instability and attachment line transition are highly important, and special attention has to be paid to these phenomena when designing laminar airfoils for swept wings.

III. Design of Natural Laminar Flow Airfoils for Swept Wings

A. Methods for Design

The most critical point when designing natural laminar flow airfoils for swept wings at high Reynolds numbers is the prediction of transition location. For low Reynolds numbers ($Re \approx 3 \cdot 10^6$) and swept angles of $\varphi = 0$ deg, very efficient empirical relations have been derived[8,9] from a large data base of experiments. For higher Reynolds numbers, only a few experiments exist to prove these criteria. For attachment line transition, empirical relations[6,7] also seem to work satisfactorily. Empirical relations for determining transition due to crossflow instability have been established.[10,11] As the experimental data base proving these criteria is very small, these relations seem not to be adequate to serve as a realistic tool in the design of high Reynolds number airfoils for swept wings. A more sophisticated approach for determining transition location is the use of the stability theory of laminar boundary layers.[1,12,13] We refer here to the work presented in Refs. 5 and 14, where a stability analysis on the basis of the temporal stability theory for boundary layers on swept wings has been described. The basic idea is the investigation of the amplification of disturbances in the form of waves within the boundary layer. The governing three-dimensional disturbance equations[15] derived from the Navier-Stokes equations can be reduced to a single quasi-two-dimensional disturbance equation in the direction of the disturbance wave front, which in the three-dimensional case is normally not in the direction of the local flow. This equation, known as the Orr-Sommerfeld-equation,[1] was derived in Ref. 15 for the direction normal to the wave front. It can be applied[15] to the three dimensional stability problem by solving a series of two-dimensional problems with various wave propagation angles. Solutions of this equation are obtained by solving an eigenvalue problem and are described in Ref. 5 by employing the computer code SALLY for incompressible, three-dimensional parallel flow.

This code allows the calculation of amplification rates of disturbance of various wave lengths, frequencies, and different disturbances propagation directions. From these amplification rates, the amplification ratio can be determined. If it is assumed that a disturbance has an amplitude A_0 when it first starts amplifying, then the amplification ratio A/A_0 at any point can be calculated by integrating the amplification rate up to that

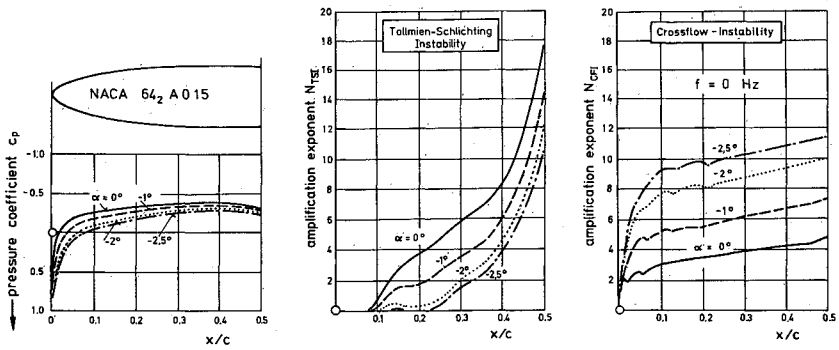

Fig. 3 Tollmien-Schlichting and crossflow instability for NACA 62_2A015 airfoil upper surface for different angles of attack, $M = 0.27$, $Re = 15 \cdot 10^6$, $\varphi = 20$ deg.

point. This amplification ratio can be expressed by an exponential function e^N, where N is the amplification exponent, or N factor. It describes the growth of the oscillations and will be related to the transition condition. This procedure must be carried out for those oscillation frequencies, wave lengths, and wave propagation directions, where the amplification exponent N becomes a maximum of all oscillations.

When analyzing the boundary layer of swept wing pressure distributions, it turns out that two principal wave front propagation directions are important. The first one is related to wing regions with weak pressure gradients, where the disturbances are propagating nearly in the direction of the outer flow, corresponding to the two-dimensional type of Tollmien-Schlichting instability. The second one is related to the wing region with strong pressure gradients near the leading edge, where the disturbances of maximum amplifications are propagating in the crossflow direction, corresponding to the crossflow instability.

Figure 3 gives an example of a stability analysis of experiments on a swept wing.[4] The left part of the figure shows the pressure distributions of a 20 deg swept wing at $M = 0.27$ and $Re = 15 \cdot 10^6$ at different angles of attack, which have been analyzed with the SALLY code[5,14] in the Tollmien-Schlichting mode, as well as in the crossflow mode. The middle part of the figure presents the amplification exponents N_{TSI} of the Tollmien-Schlichting instability as an envelope of various frequencies investigated along the wing chord. TS instability first starts a certain distance from the leading edge (approximately 8% of local chord), after which N_{TSI} increases steadily. In the right part of the figure, amplification exponents due to crossflow instability N_{CFI} have been plotted for a frequency of zero. These describe stationary waves which have also been detected in experiments. Here one can see that the amplification of the disturbances starts immediately at the leading edge and shows a steep increase in the region of large pressure gradients. Where the pressure distribution has weak gradients only a small increase in values of N_{CFI} can be seen. In the calculation with the SALLY code, no interaction between crossflow and Tollmien-Schlichting instability can be taken into account.

The usual way to proceed from these stability analysis results to the transition location is to determine the calculated N factors at the experimental transition locations, thus establishing a limiting N value. The various N factors for transition from different publications and experiments do not show a clear picture.[16-18] It seems reasonable that TS-instability transition is likely to occur at $N_{TSI} = 11$ in low turbulence wind tunnels and $N_{TSI} \approx 18$ in flight experiments.

The crossflow N values in wind tunnels reach values of $N_{CFI} \approx 9$–11[5,16] and no real flight data are available. For our following design examples, $N_{TSI} = 18$ and $N_{CFI} = 12$ have been assumed. The airfoil design has been carried out by a combined procedure using the subsonic design method of Eppler/Somers,[18] together with a modified version of the BGKJ code.[19] The transition location at the critical points was checked with the SALLY code, as previously described.

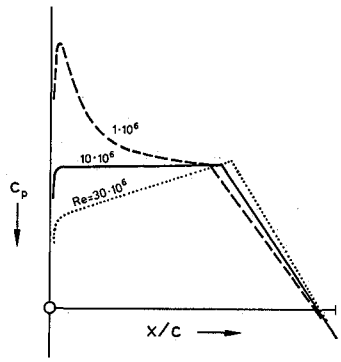

Fig. 4 Limit pressure distributions for laminar flow for different Reynolds numbers (unswept wing).

B. Design Features

The drag of a laminar flow airfoil mainly depends on the extent of the laminar boundary layer on both airfoil surfaces. Thus the aim of the design process is to get a large extent of the laminar boundary layer, while taking also into account the other design objectives and the different off-design conditions occurring on transport aircraft.[20] The extent of laminar flow on a swept wing is limited by three different mechanisms of transition into turbulent flow, as described above. For each of these three instability modes, certain differing types of favorable pressure distributions exist. In order to get a good compromise pressure distribution, it is of basic interest to investigate the influence of the pressure distribution on the different types of instability.

Figure 4 shows the limit pressure distribution of an unswept wing for different Reynolds numbers for Tollmien-Schlichting instability. Transition is prescribed to occur at the beginning of the steep pressure rise at nearly 60% of chord length for the three pressure distributions. At low Reynolds numbers the laminar flow is able to overcome a certain pressure rise. At constant pressure the transition Reynolds number in free flight may have values of 5–8 million, indicated by a chord length Reynolds number of 10 million in Fig. 4. At higher Reynolds numbers the flow has to be more and more accelerated to keep the boundary layer laminar.

Additionally, the shape of the pressure distribution has a strong influence on transition behavior. Figure 5a shows a conventional convex pressure distribution in comparison with a more front-loaded one. The front-loaded pressure distribution induces remarkably higher amplification rates of TS waves in the forward part of the laminar flow region, but near the pressure minimum it results in a lower amplification ratio than the conventional type, as shown in Fig. 5b.

If the amplification ratio curve of the front-loaded type reaches the limiting line at which transition is assumed to oc-

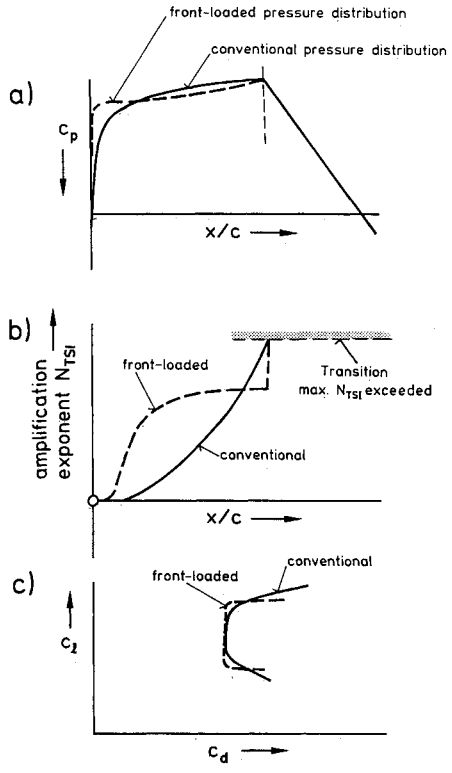

Fig. 5 Effect of pressure distribution on amplification exponent N_{TSI} and drag polar (unswept wing): a) pressure distributions; b) amplification exponents N_{TSI}; c) drag polars.

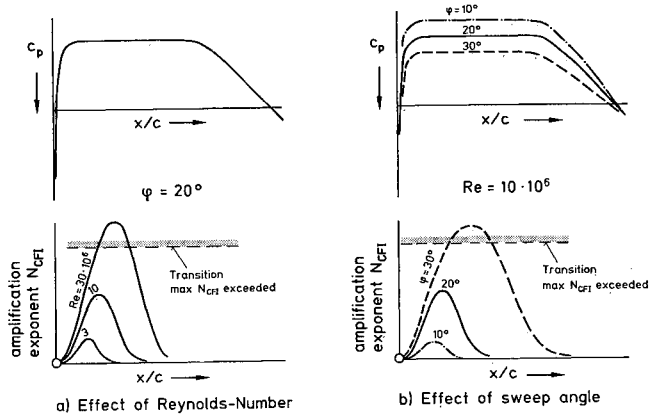

Fig. 6 Effects of Reynolds number and sweep angle on amplification exponent N_{CFI} (swept wing).

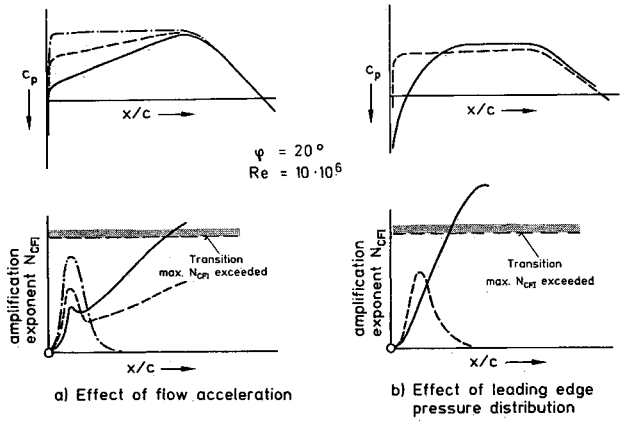

Fig. 7 Effect of flow acceleration and leading edge pressure distribution on amplification exponent N_{CFI} (swept wing).

cur, the transition location moves rapidly upstream. For the conventional pressure distribution, the transition location is moving slowly upstream with increasing angle of attack, but it has already started moving at lower angles of attack. This different transition behavior leads to different types of laminar drag buckets, as shown in the drag polar curve in Fig. 5c. The front-loaded type of pressure distribution has a larger range of lift coefficients with minimum drag, but this range is limited by a steep drag increase. In the case of the conventional pressure distribution, the laminar drag bucket is more rounded.

On swept wings the choice of sweep angle depends on the crossflow instability. The steep pressure drop at the leading edge produces large crossflow velocities with large amplification ratios, as shown in Fig. 6a. In the following region of constant pressure no spanwise pressure gradients exist. Thus, the crossflow velocities disappear and so does the instability. With increasing Reynolds number, the amplification ratio grows until at least a certain limiting N factor is reached and transition occurs.

The effect of sweep angle can be seen in Fig. 6b. With increasing sweep angle the pressure drop is reduced, but because of the increasing crossflow component the amplification ratio becomes larger.

The effect of a slight flow acceleration downstream of the steep leading edge pressure drop is given in Fig. 7a. Near the leading edge the N factor grows rapidly, due to the steep pressure drop. In the following region of slight acceleration, the N factor decreases and then farther downstream slightly increases again. This is caused by different wavelengths.

Figure 7b shows the influence of leading edge pressure distribution on the growth of crossflow waves. The more rounded type, designated as conventional pressure distribution, induces an increasing amplification ratio in the whole laminar flow region. The more front-loaded pressure distribution at first shows a stronger growth of the amplification ratio, but farther downstream the crossflow becomes stable, due to the nearly constant pressure. It is remarkable that the maximum amplification ratio of the front-loaded pressure distribution is clearly lower than that of the conventional one.

On a wing, the possibility of transition by Tollmien-Schlichting instability and crossflow instability leads to a transition behavior, as shown in Fig. 8, where the chordwise transition location is plotted vs lift coefficient for the upper and lower surface. Starting from the design lift coefficient in the middle of the laminar bucket of an unswept wing in Fig. 8a, the upper limit of the laminar bucket is given by the upstream moving transition location on the upper surface at increasing angles of attack. The lower limit is given by the transition location on the lower surface at decreasing angles of attack. Figure 8b shows that in the case of a swept wing each surface has its own laminar bucket. On the upper side, for example, the upper limit is given in the same manner as that described in Fig. 8a. The lower limit is given by crossflow induced transition, which is caused by the increasingly rounded leading edge pressure distribution, with decreasing angles of attack. In a similar way, a laminar bucket for the lower surface can be constructed. The upper limit is given by transition due to crossflow instability, while the lower limit results from a transition by a Tollmien-Schlichting instability. On a well-designed airfoil, the laminar buckets of both sides should have the same limits of lift coefficient.

Lastly, the mechanism of attachment line transition has to be taken into account. Following the criterion mentioned in Sec. III-A and given in Refs. 6 and 7, the attachment line transition will be forced by large sweep angles, large Reynolds numbers, and small flow acceleration at the leading edge.

The same design features which prevent transition by crossflow instability seem also to be favorable to prevent at-

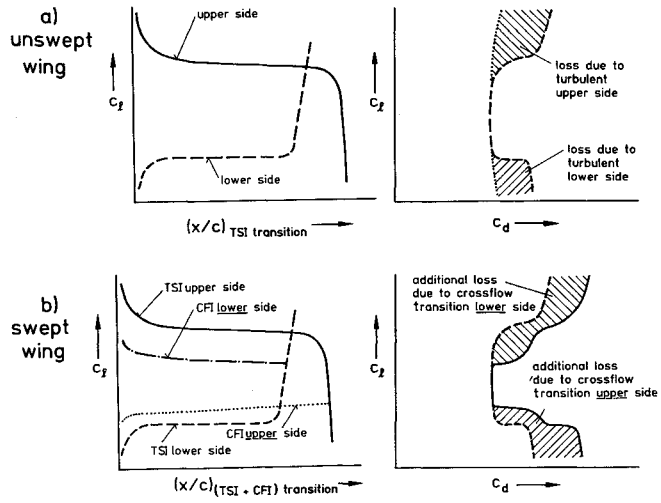

Fig. 8 Position of transition and schematic drag development as function of lift. a) unswept wing: transition due to TSI; b) swept wing: transition due to TSI and CFI.

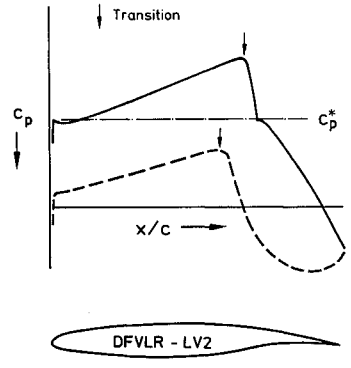

Fig. 9 Pressure distribution and shape of transonic laminar airfoil DFVLR-LV2.

tachment line transition. The airfoil calculations presented in this paper indicate that the attachment line transition does not occur if the transition by crossflow is prevented.

Combining the design features of TSI, CFI, and ALT, the following arrangement of the pressure distribution seems to be necessary for a natural laminar flow airfoil for transport aircraft with swept wings: steep pressure distribution at the leading edge (favorable for CFI and ALT), followed by a small region of constant pressure or even a slight, small pressure rise (favorable for CFI), followed by a concave pressure distribution with slight acceleration until the steep pressure rise with turbulent boundary layer (favorable for TSI).

C. Design Objectives and Airfoil Design

The design objectives for a transport aircraft wing are given by the following values: flight Mach number $M_F = 0.8$; Reynolds number $Re = 30 \cdot 10^6$; sweep angle $\varphi = 22°$; lift coefficient $c_L = 0.5$. This leads to the design values of a basic airfoil with $M = 0.74$; $Re = 26.5 \cdot 10^6$; and $c_l = 0.6$.

Taking into account these design objectives and the design features described in Sec. III-B, a natural laminar airfoil, DFVLR-LV2, was designed with a thickness of 11.7%.[21,22] The pressure distribution is shown in Fig. 9. The laminar flow is extended through 65% of chord length on the upper surface and 60% on the lower surface. The supersonic field on the upper surface is closed by a weak shock. The shock strength is

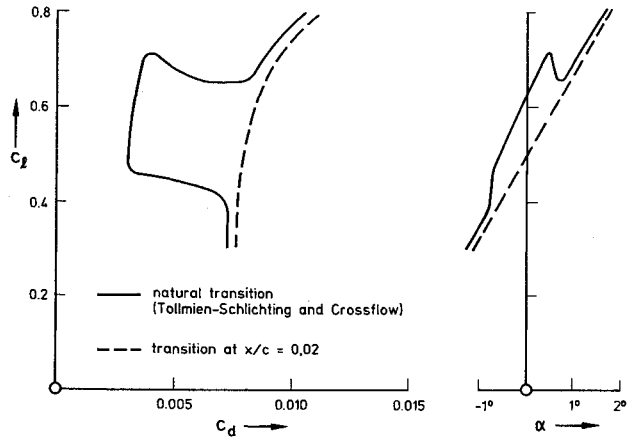

Fig. 10 Calculated lift and drag coefficients of airfoil DFVLR-LV2 at $M = 0.74$, $Re = 26.5 \cdot 10^6$ and $\varphi = 22$ deg.

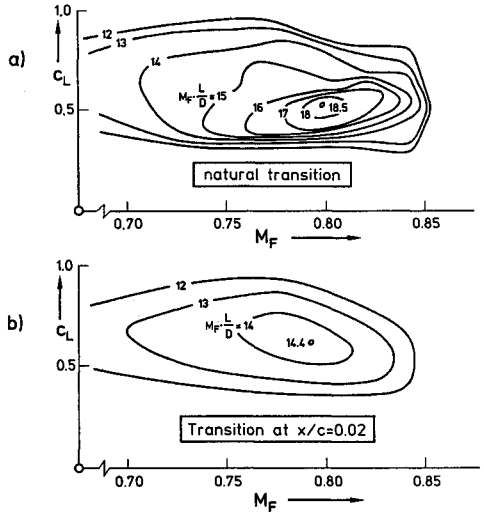

Fig. 11 Performance $M_F \cdot L/D$ of a transonic transport aircraft with DFVLR-LV2 airfoil wing and sweep angle $\varphi = 22$ deg: a) natural transition; b) transition fixed.

so small that the calculations do not give an additional wave drag.

Figure 10 shows calculated drag and lift coefficient polar curves at the design Mach number $M = 0.74$, taking into account transition due to Tollmien-Schlichting instability, as well as crossflow instability. The transition location in these calculations is given by the SALLY code, with an assumed maximum amplification exponent of $N_{TSI} = 18$ for Tollmien-Schlichting waves and $N_{CFI} = 12$ for crossflow waves. At the upper limit of the laminar bucket, the upper surface becomes turbulent by TSI and the lower surface by CFI, whereas at the lower limit the lower surface becomes turbulent by TSI and the upper surface by CFI. The calculations give a minimum drag of $c_d = 0.0036$ and a width of the laminar bucket of $\Delta c_l \approx 0.2$. By means of a simple flap the bucket can be shifted to higher or lower lift coefficients. In comparison to this natural laminar flow behavior, the corresponding drag polar for the airfoil, with fixed transition at 2% chord length, shows a remarkable increase in drag coefficient.

The lift coefficient vs angle-of-attack curve shows a strange behavior in the case of the natural laminar flow airfoil.

The lift curve slope inside the laminar bucket is steeper than outside the bucket. This behavior is caused by the thinner boundary layer. The rapidly changing boundary-layer thickness at the limits of the laminar bucket causes a very steep slope

Table 1 Drag coefficients of fuselage, empennage, nacelle, and miscellaneous

Drag	Conventional aircraft	Contaminated laminar aircraft	Clean laminar aircraft
Additional drag of slat	0.0005	0	0
Empennage	0.0032	0.0032	0.0014
Fuselage	0.0070	0.0070	0.0070
Nacelle	0.0002	0.0002	0.0002
Miscellaneous	0.0010	0.0010	0.0010
C_D parasite	0.0119	0.0114	0.0096

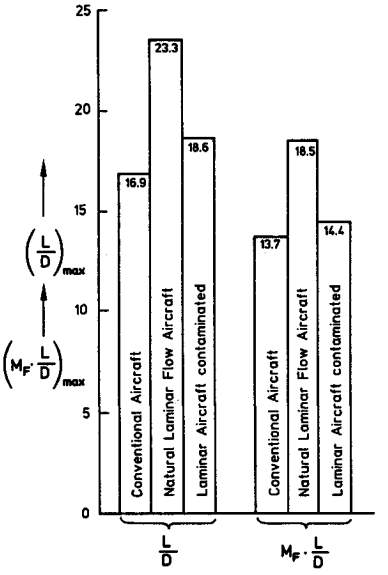

Fig. 12 Comparison of L/D and performance $M_F \cdot L/D$ of conventional aircraft and natural laminar flow aircraft.

near the lower limit and an adverse slope near the upper limit. These typical discontinuities may cause problems in guidance and control of an aircraft.

IV. Effect of Natural Laminar Flow Airfoils on Aircraft Performance

In order to judge the benefits of laminar airfoils, one has to investigate their consequences on aircraft performance. The performance of an aircraft can roughly be described by the ratio L/D times flight Mach number M_F. The ratio L/D represents the aerodynamic efficiency of the aircraft, i.e., the fuel consumption for a given flight distance, while the flight Mach number M_F takes into account the flight time. For comparison, these values have been determined in Refs. 21 and 22.

On the basis of the drag polars in Fig. 10, the aircraft performance data have been calculated for clean and contaminated laminar airfoils, including the induced drag and the drag of the empennage and fuselage. The airfoils of the empennage have also been assumed to be laminar. The used drag coefficients of fuselage and empennage are given in Table 1.

In order to convert the airfoil data to wing data using simple sweep theory, the airfoil lift coefficients are multiplied by the square of cosine of the sweep angle, whereas the drag coefficients remain unchanged. The flight Mach number is the airfoil Mach number divided by cos φ. The considered transport aircraft is of an Airbus-type and has a wing with a sweep angle of $\varphi = 22$ deg and an aspect ratio of $\Lambda = 8.8$.

Figure 11 presents two c_L-M_F diagrams with lines of constant performance $M_F \cdot L/D$ for comparing two essential cases: the "laminar aircraft" equipped with laminar wing and empennage (laminar boundary layer through 65% chord on wing upper surface and 60% on lower surface) and turbulent fuselage, and an aircraft with contaminated wing and empennage (boundary layer transition assumed at 2% chord for both surfaces). For the latter, there are smooth closed curves of constant $M_F \cdot L/D$ around a maximum value of $(M_F \cdot L/D)_{max} = 14.4$ at a Mach number of $M_F = 0.8$. Similar results (not shown) have been obtained for an aircraft with conventional wing and empennage. The wing is assumed to have the same weight as the laminar wing and, therefore, the wing sweep and the wing thickness are higher and the aspect ratio is lower. For the "laminar aircraft," the curves are not so smooth, as a consequence of the drag polar of the laminar airfoil in Fig. 10, but show an essentially higher maximum of $(M_F \cdot L/D)_{max} = 18.5$ at a Mach number $M_F = 0.8$. This latter value demonstrates very clearly the remarkable improvement in performance of an aircraft with laminar wing and empennage.

A comparison of the maximum value of L/D and $M_F \cdot L/D$ for a conventional aircraft and the two cases of an aircraft with clean and contaminated laminar wing and empennage is given in Fig. 12. According to this, the contaminated "laminar aircraft" is still a little more beneficial than the conventional aircraft. But one has to keep in mind that the cruise Mach number of the conventional aircraft is slightly higher. On the contrary the clean "laminar aircraft" shows about 30% improved values of L/D (fuel consumption for a given distance) and $M_F \cdot L/D$ (performance) compared with the conventional one.

V. Problems Associated with Laminar Flow on Wings and Experimental Verification

Before realizing a laminar flow aircraft, a set of problems has to be solved. The most critical and important one is the reliable prediction of transition location on wings in free flight at high Reynolds numbers.

It was pointed out in Sec. III that, with the aid of the stability analysis of laminar boundary layers, a transition location may be predicted by relating measured transition locations with calculated amplification ratios and hence defining limiting values of N factors for Tollmien-Schlichting instability, as well as for crossflow instability. These limit values can only be derived from suitable and accurate experiments in free flight and wind tunnels.

Figure 13 shows the results of such an analysis, with respect to Tollmien-Schlichting instability for published flight tests and wind tunnel experiments in the Reynolds number range $Re = 3 \cdot 10^6$–$40 \cdot 10^6$.[23] The amplification exponents N_{TSI} obtained from free flight tests at Reynolds numbers of 9–15 $\cdot 10^6$ are of the order of $N_{TSI} = 20$, whereas the values of N_{TSI} from low turbulence wind tunnel experiments at Reynolds numbers 17–40 $\cdot 10^6$ lie between $N_{TSI} = 10$ and 13. Essentially lower values have been obtained from blowdown wind tunnel tests at Reynolds numbers of 3–6 $\cdot 10^6$. These values are only of the order of $N_{TSI} \approx 3$.

One possible reason for the difference between the found amplification exponents from free flight and wind tunnel tests is that microturbulence and noise in wind tunnel flow are always present and dependent on the construction of the wind tunnel and the achieved flow quality. As a laminar boundary layer is strongly influenced by turbulence and noise, premature

boundary-layer transition in wind tunnels is observed. This can be confirmed by comparing the results of the limiting N_{TSI} factors in blowdown wind tunnels, in which appreciably smaller N_{TSI} values occur, due to higher levels of turbulence and noise, with those in continuous low turbulence wind tunnels. These wind tunnel problems become evident in Fig. 14, which presents a comparison of one calculated and two measured drag polars for the laminar airfoil DFVLR-LV2 (unswept case). (The calculations have been described in Sec. III-C.) The experiments have been carried out at DFVLR in the Transonic Wind Tunnel in Braunschweig (TWB),[24] with free transition at Reynolds numbers $Re = 3 \cdot 10^6$ and $6 \cdot 10^6$. For both Reynolds numbers the curves show a laminar bucket with considerably smaller drag coefficients compared with those which one would expect with a fully turbulent boundary layer. But with increasing Reynolds numbers, the bucket width decreases. At $Re = 9 \cdot 10^6$, the laminar bucket has disappeared (values not shown) but the calculation indicates that even at $Re = 26.5 \cdot 10^6$ the laminar bucket with a width of $\Delta c_l = 0.2$ should exist. These experiments indicate quite clearly that it is possible to produce laminar boundary layers on airfoils at higher subsonic Mach numbers in this kind of wind tunnel, with pressure gradients which can be used for laminar airfoils at high Reynolds numbers. But it is also clear that the amplification exponents N_{TSI} derived from these experiments (see Fig. 13) are too small to allow long laminar boundary layers with corresponding low drag coefficients and wide laminar buckets at Reynolds numbers necessary for transport aircraft. The results in Figs. 13 and 14 underline that it is absolutely necessary to have transonic wind tunnels with a high flow quality, reliable and accurate free flight tests, and a correlation with respect to transition between wind tunnel and free flight.

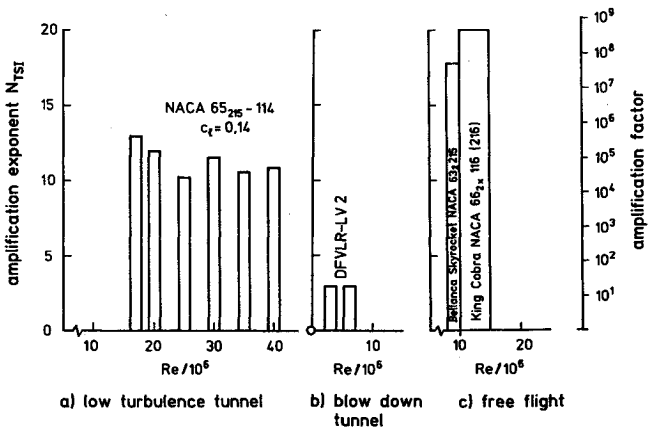

Fig. 13 Limit amplification exponents for TSI derived from free flight and wind tunnel experiments.

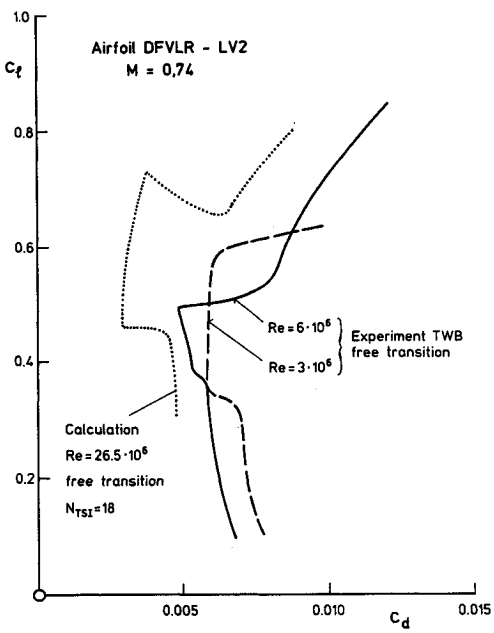

Fig. 14 Calculated and measured drag polars of airfoil DFVLR-LV2 (unswept case).

Besides the problem of airfoil development and experimental verification, further difficulties exist which should be briefly mentioned here:

1) Replacement of slats by a more efficient trailing edge flap system.

2) Problems with engine noise interaction with the laminar boundary layer.

3) Smooth wing surface and small waviness.

4) Contamination of the wing by insects and dust.

With respect to roughness (waviness, smoothness, contamination), theoretical considerations show that the permissible absolute height of surface roughness of transport aircraft wings has about the same order as sailplanes. This is due to nearly the same unit Reynolds number for sailplanes and for transport aircraft flying at high altitudes. Operational experiences with sailplanes through the years indicate that, despite insect contamination, the advantages of laminar airfoils have been proven.

VI. Conclusions

Summarizing the results of the present paper, the following statement can be made:

1) The design of natural laminar flow airfoils for high Reynolds numbers and swept wings seems to be possible.

2) Performance of transport aircraft with laminar wing and empennage is improved by 30%, compared to the performance of a conventional aircraft.

3) The assumptions leading to these statements have to be validated with respect to transition prediction and experimental verification; therefore, suitable and reliable flight experiments have to be conducted at high Reynolds and Mach numbers.

4) Transonic wind tunnels with high flow quality are indispensable.

References

[1]Schlichting, H., *Boundary-Layer Theory*, 7th ed. McGraw-Hill, New York, 1979.

[2]Gray, W. E., "The Effect of Wing Sweep on Laminar Flow," RAE TM Aero. 255, 1952.

[3]Owen, P. R. and Randall, D. J., "Boundary Layer Transition on the Sweptback Wing," RAE TM Aero. 277, 1952.

[4]Boltz, F. W., Kenyon, G. C., and Allen, C. Q., "Effects of Sweep Angle on the Boundary-layer Stability Characteristics of an Untapered Wing at Low Speeds," NASA TN-D 338, 1960.

[5]Skrokowski, A. J. and Orzag, S. A., "Mass Flow Requirements for LFC Wing Design," AIAA Paper 77-1222, 1977.

[6]Pfenninger, W., "Laminar Flow Control; Laminarization," AGARD-R-654, 1977, pp. 3–1 to 3–75.

[7]Poll, D. I. A., "Transition in the Infinite Swept Attachment Line Boundary Layer," *The Aeronautical Quarterly*, Vol. 30, 1979, pp. 607–629.

[8]Granville, P. S., "The Calculation of the Viscous Drag of Bodies of Revolution," David Taylor Model Basin Report 849, 1953.

[9]Michel, R., "Critère de Transition et Amplification des Ondes d'Instabilité Laminaire," *La Recherche Aérospatiale*, No. 70, 1979.

[10]Beasley, J. A., "Calculation of the Laminar Boundary Layer and the Prediction of Transition on a Sheared Wing," ARC R&M 3787, 1973.

[11]Arnal, D., Habiballah, M., and Coustouls, E., "Laminar Instability Theory and Transition Criteria in Two- and Three-dimensional Flow," *La Recherche Aérospatiale*, No. 1984-2, 1984.

[12]Betchov, R. and Criminale, W. O., *Stability of Parallel Flows*, Academic Press, New York, 1967.

[13]Mack, L. M., "Boundary Layer Stability Theory," JPL Rept. 900-277, Rev. A., 1969.

[14]Dagenhardt, J. R., "Amplified Crossflow Disturbances in the Laminar Boundary Layer on Swept Wings with Suction," NASA TP 1902, 1981.

[15]Gregory, N., Stuart, J. W., and Walker, W. S., "On the Stability of Three-dimensional Boundary Layer with Application to the Flow Due to a Rotating Disc," *Philosophical Transactions of the Royal Society of London*, Series A, No. 943, Vol. 248, 1955, pp. 155–199.

[16]Runyan, J. and George-Falvy, D., "Amplification Factors at Transition on an Unswept Wing in Free Flight and on Swept Wing in Wind Tunnel," AIAA Paper 79-0267, 1979.

[17]Jaffe, N. A., Okamura, T. T., and Smith, A. M. O., "Determination of Spatial Amplification Factors and Their Application to Predicting Transition," *AIAA Journal* Vol. 8, 1970, pp. 301–308.

[18]Obara, C. J. and Holmes, B. J., "Flight-measured Laminar Boundary-Layer Transition Phenomena Including Stability Theory Analysis," NASA TP 2417, 1985.

[19]Rohardt, C. H., "Erweiterung eines Nachrechnungsverfahrens für zweidimensionale Strömungen durch ein leistungsfähiges Grenzschichtverfahren," DFVLR-IB, 1983.

[20]"Hybrid Laminar Flow Control Study, Final Technical Report," Boeing Commerical Airplane Co., NASA CR 165930, 1982.

[21]Horstman, K. H., Köster, H., Redeker, G., and Quast, A., "Laminarprofile für Verkehrsflugzeuge," DFVLR-IB, 1985.

[22]Horstmann, K. H., Köster, H., Redeker, G., and Quast, A., "Der Laminarflügel—Ein Weg zur Verbesserung der Wirtschftlichkeit von Verkehrsflugzengen," *DFVLR-Nachrichten*, Heft 46, 1985.

[23]Rohardt, C. H., "Anwendung eines Berechnungsverfahrens zur Ermittlung der Instabilitäten in der laminaren Grenzschicht im Hinblick auf die Bestimmung des laminar-turbulenten Umschlags an Profilen," DFVLR-IB, 1983.

[24]Stanewsky, E., Puffert-Meissner, W., Müller, R., and Hoheisel, H., "Der Transsonische Windkanal Braunschweig der DFVLR," *Z. Flugwiss. Weltraumforsch.*, Vol. 6, 1982, pp. 398–408.